Journal of Applied Physics

Crystallization properties of melt-quenched Ge-rich GeSbTe thin films for phase change memory applications

Cite as: J. Appl. Phys. **128**, 155105 (2020); https://doi.org/10.1063/5.0023696
Submitted: 31 July 2020 . Accepted: 28 September 2020 . Published Online: 16 October 2020

S. M. S. Privitera, I. López García, C. Bongiorno, V. Sousa, M. C. Cyrille, G. Navarro, C. Sabbione, E. Carria, and E. Rimini

Journal of Applied Physics ARTICLE scitation.org/journal/jap

Crystallization properties of melt-quenched Ge-rich GeSbTe thin films for phase change memory applications

Cite as: J. Appl. Phys. **128**, 155105 (2020); doi: 10.1063/5.0023696
Submitted: 31 July 2020 · Accepted: 28 September 2020 ·
Published Online: 16 October 2020

S. M. S. Privitera,[1,a)] I. López García,[1] C. Bongiorno,[1] V. Sousa,[2] M. C. Cyrille,[2] G. Navarro,[2] C. Sabbione,[2] E. Carria,[3] and E. Rimini[1]

AFFILIATIONS

[1]Institute for Microelectronics and Microsystems, National Research Council (IMM-CNR), Zona Industriale Ottava Strada 5, 95121 Catania, Italy
[2]CEA-LETI, MINATEC Campus, 17 avenue des Martyrs, F-38000 Grenoble, France
[3]STMicroelectronics, Stradale Primosole 50, 95121 Catania, Italy

Note: This paper is part of the Special Topic on Phase-Change Materials: Syntheses, Fundamentals, and Applications.
[a)]**Author to whom correspondence should be addressed:** stefania.privitera@imm.cnr.it

ABSTRACT

The crystallization process of melt quenched Ge-rich GeSbTe films, with composition optimized for memory applications, has been studied by optical reflectance measurements. The optical properties have been related to the structure and composition by means of the effective medium approximation. The compositional variations have been investigated by transmission electron microscopy and electron energy loss spectroscopy. Amorphous materials prepared by melt-quenching with different laser energy densities have been studied. For the energy density of 1.5 J cm^{-2}, a uniform amorphous layer, with embedded Ge crystalline grains, is obtained. The film exhibits a crystallization temperature of 275 °C and no relevant phase separation during crystallization. For a lower energy density of 1 J cm^{-2}, only half of the film thickness is quenched to the amorphous phase, with Ge depletion. The crystallization temperature of the Ge depleted film is 245 °C, and a partial phase separation occurs.

INTRODUCTION

One of the most promising non-volatile memory technologies is based on phase change materials (PCMs). PCMs are the heart of optical storage technologies since amorphous and crystalline phases display strong optical contrast along with fast and reversible switching between those two states. The large variation in optical reflectivity is accompanied by an even larger variation in resistivity, therefore enabling the realization of non-volatile memory.[1,2] In conventional devices, switching between the crystalline and amorphous states is obtained by applying a short, high-energy electrical pulse that melts the PCM followed by a rapid thermal quench, producing the amorphous phase (RESET operation). The crystalline phase is formed via a longer, lower-energy electrical pulse, which crystallizes the material (SET operation). The reading operation is performed at a low voltage by reading the current and determining the high (RESET) or low resistance (SET) state. This technology is already in production in the 20 nm node and moves toward the 10 nm node. More recently, the technological importance of PCMs dramatically increased since it has the potential to dominate the storage class memory (SCM), an intermediate step between high-performance DRAM and low-cost nonvolatile memory, combining persistence and speed in the same device.[3] However, several challenges still need to be addressed and solved. Among these, the low data retention represents a crucial aspect, especially for automotive applications. Indeed, the commonly adopted materials are Ge–Sb–Te (GST) alloys, which exhibit crystallization temperature around 150 °C. This means that operation at high temperatures (>150 °C) for a long period, as required for the automotive market,

cannot be guaranteed. Several PCMs working at a temperature compatible with automotive applications have also already been selected.[4–6] Despite the introduction of different dopant species, from nitrogen to carbon in GST,[7,8] no ultimate solution to the thermal instability of GST is currently available; this kind of issue also involves the soldering reflow, during which the tendency to crystallization at the process temperatures is critical for code integrity; in this respect, a Ge-rich GST alloy featured by a crystallization temperature of 370 °C has been reported, although the set speed is decreased by a factor 3.7. Over the last few years, Ge-rich materials have been optimized in terms of cyclability, drift, and speed. However, their tendency to decompose still calls for investigation on the basic mechanisms leading to element diffusion and compositional variations. In the particular case of Ge-rich GST, it has been shown that during the initial seasoning procedure, Ge segregates at the periphery of the liquid zone,[5] impoverishing the melted volume. Such a stoichiometry modification seems to occur only during the initialization process, leading to a stable active cell. It has been shown that the Ge segregation outside the liquid volume is essentially due to the high Ge diffusion coefficient in the melted material (of the order of 10^{-5} cm^2/s),[9] and it occurs even in the absence of an applied electric field. Therefore, atomic diffusion, with the subsequent stoichiometry variation, may be a factor playing a relevant role in the endurance, especially when the device is made by two different compositions and operates at high temperatures. For this reason, the crystallization of the as deposited amorphous film, characterized by the formation of pure Ge crystalline grains as studied recently,[10] may be markedly different in the case of melt quenched materials in which Ge atoms tend to segregate outside the liquid zone.

In order to investigate the material stability, in this paper we study the crystallization properties of Ge-rich films after laser melting and quenching at different energy density, i.e., after amorphization of different volumes of material, as well as different degrees of Ge segregation. Correlation of the optical properties with high resolution transmission electron microscopy and energy loss spectroscopy gives the possibility to clarify the compositional variations upon crystallization by thermal annealing.

EXPERIMENTAL METHODS

Ge-rich GeSbTe films have been sputter deposited on 8 in. Si (100) wafer using a $Ge_2Sb_2Te_5$ (GST225) target together with a pure Ge target in a mixture of Ar and N_2 as sputtering gas. The addition of nitrogen has the twofold aim of reducing the oxidation of the PCM film during the fabrication since it bonds to Ge,[11] which is the core oxidizing species, and to enable a finer grain structure, which has been shown to be beneficial for the device yield.[12] The thickness of the deposited film is 40 nm and the composition is equivalent to a $Ge_2Sb_2Te_5$ film with 45 at. % excess Ge and 4 at. % N. The film is deposited in the amorphous phase and covered by a 5 nm thick Si oxide layer. After deposition, annealing at 400 °C converted the film in the crystalline structure. During this annealing, partial segregation of the excess Ge occurs, with the formation of pure Ge crystalline grains with a grain size of about 10 nm.[5,9]

The film was then irradiated by a 600 ns pulsed Yb-YAG laser (515 nm) with a frequency of 10 kHz. A shot-by-shot stepping approach is used to process the whole 8 in. wafer surface, employing a motorized chuck. The laser emits with a Gaussian shape but, for our purposes, the optical path has been designed in such a way to obtain a rectangular beam that shows a Gaussian shape on one axis (x) and top-hat shape on the other one (y), obtained with the use of a homogenizer. The short x axis, with a nearly Gaussian profile, has a FWHM of 30.0 μm ± 0.1 μm. The long y axis, with top-hat shape, is higher than 98% in a region of 3.000 mm ± 0.001 mm. The geometry of the laser beam has been monitored via software by a CCD camera mounted on the chuck and the chuck scanning velocity has been chosen in order to achieve uniform processing of the wafer. The laser power P on the samples has been measured by a power-meter mounted on the chuck. The corresponding energy density F is given by the power, measured by the power-meter, divided by the beam area (0.03 × 3 mm^2) and by the number of pulses per second.

Two energy density values have been employed: 1 J/cm^2 and 1.5 J/cm^2. Below 1 J/cm^2, no variation in the reflectivity signal has been observed. Above 1.5 J/cm^2, film ablation occurred.

As reported in previous work,[9] irradiation using 1 J/cm^2 as energy density produces amorphization of a 20 nm thick surface layer and outdiffusion of Ge from the liquid. As a consequence, after melting and quenching, the bottom part of the film (20 nm thick) is crystalline with a higher Ge content, while the upper part (20 nm) is amorphous, with a lower Ge content. This sample will be indicated in the following as L1.

Upon irradiation at 1.5 J/cm^2, the entire film thickness is melted and quenched, with the exception of the pure Ge grains (because of the higher melting temperature of Ge). The Ge content appears to be more distributed in the amorphous phase. This sample is mentioned in the following as L2. A schematic of the samples is shown in Fig. 1. On the right, a picture shows several regions of the same wafer after irradiation at different fluences or in the as prepared crystalline state. The melting and quenching is associated with a decrease of the reflectivity, which makes the film darker in the irradiated regions. In the L2 sample, the reflectivity decreases more than in L1.

After melting and quenching, L1 and L2 samples were annealed under 3 min isochronal anneals up to 300 °C, to determine the crystallization temperature. The reflectivity was measured *in situ*, during annealing, using a laser with a wavelength of 790 nm and a Si photodiode. The laser wavelength has been chosen to maximize the reflectivity contrast between amorphous and crystalline phase. The incidence angle is 68°.

The structure and the composition of the film upon different annealing temperatures have been studied *ex situ* by TEM and STEM, coupled to EELS mapping, by using a JEOL JEM 2010F electron microscope with a 200 kV accelerating voltage.

RESULTS AND DISCUSSION

Figure 2(a) shows the reflectivity obtained by measuring the current of a photodiode upon reflection of the laser beam at the Ge- rich GST sample surface. The reflectivity has been obtained from the photocurrent by calibration using a gold mirror. Measurements have been performed *in situ*, during subsequent annealing treatments at increasing temperature, for 3 min.

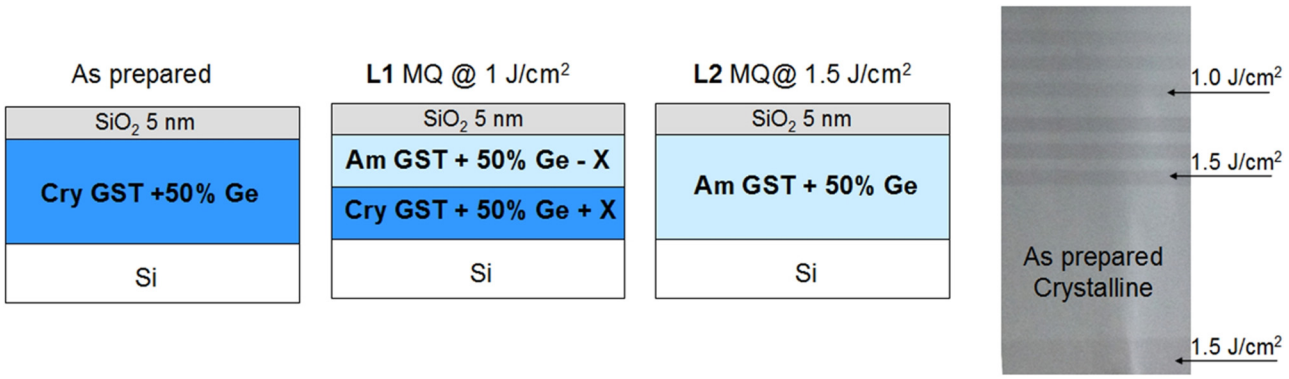

FIG. 1. Schematic of the samples. On the right, the optical picture of different regions of the same wafer irradiated at different fluences or in the as prepared crystalline state. The reflectivity contrast upon amorphization is clearly visible.

Sample L1, after melting and quenching at low fluences, has a 20 nm thick amorphous layer on top of 20 nm crystalline film and exhibits a reflectivity higher than the sample L2. Upon annealing, at temperatures higher than 230 °C, the reflectivity increases due to the crystallization process.

The crystallization temperature can be evaluated as the temperature at which the first derivative of the reflectivity vs temperature exhibits a maximum. In this way, we obtain 245 °C and 275 °C for the samples L1 and L2, melt quenched at low (1 J/cm^2) and high energy density (1.5 J/cm^2), respectively.

MODELING

The reflectivity of inhomogeneous materials, as a Ge-rich GST film, can be evaluated by considering the effective medium approximation developed by Bruggeman,[13] to describe the optical and electrical properties of layers with two coexistent phases (either two different compositions or crystalline and amorphous phase with the same composition). Reference 14 describes how to calculate the dielectric function ε_{eff} for various shapes of composite materials as a function of the "dopant" (ε_d) and the host material properties (ε_0). In the case of materials made by spherical clusters embedded in a matrix with different compositions,

$$\varepsilon_{eff} = 1/4[2\varepsilon_p - \varepsilon'_p + \sqrt{[(2\varepsilon_p - \varepsilon'_p)^2 + 8\varepsilon_0\varepsilon_d}], \quad (1)$$

with $\varepsilon_p = (1-f)\varepsilon_0 + f\,\varepsilon_d$ and $\varepsilon'_p = f\varepsilon_0 + (1-f)\,\varepsilon_d$.

In the case of Ge-rich GST, the "dopant" is Ge and the host matrix is GST225.

Since the film is deposited on Si(100) and coated by a thin SiO_2 layer, the reflectivity of the entire stack is the resultant

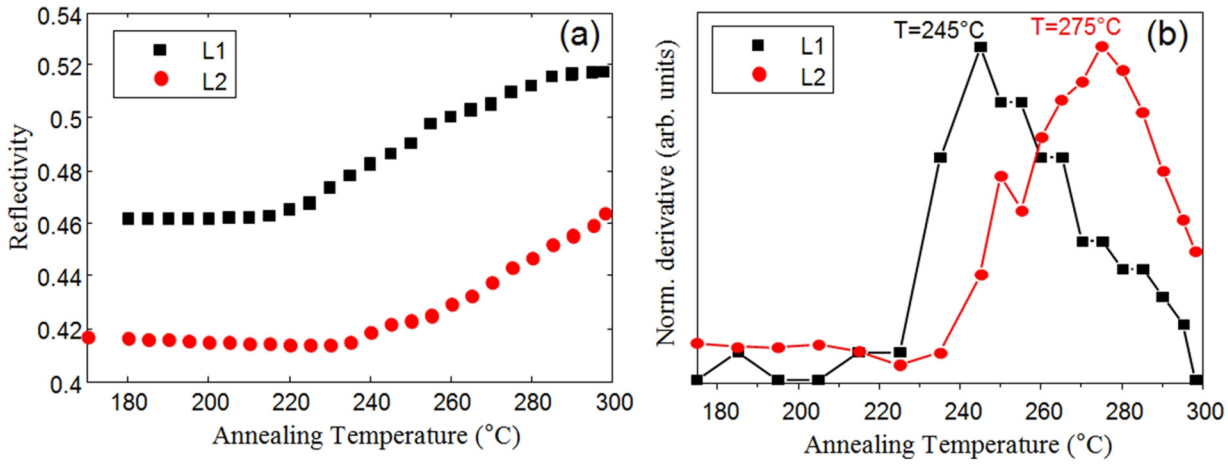

FIG. 2. (a) Reflectivity vs temperature during isochronal annealing (3 min). (b) Derivative of the reflectivity vs temperature.

reflectance, that can be obtained using the matrix approach

$$M = M_{SiO_2} M_{GST}. \quad (2)$$

In general, M_j is a 2×2 matrix representing the jth film of the system, with refractive index n_j and thickness d_j

$$M_j = \begin{pmatrix} \cos\delta_j & \frac{i}{\eta_j}\sin\delta_j \\ i\eta_j \sin\delta_j & \cos\delta_j \end{pmatrix}, \quad (3)$$

where the effective optical thickness δ_j, for an angle of refraction θ_j, is

$$\delta_j = \frac{2\pi}{\lambda} n_j d_j \cos(\theta_j). \quad (4)$$

In Eq. (3), η_j is the effective refractive index of the layer, equal to $n_j/\cos\theta_j$ for the p-polarization and to $n_j \cos\theta_j$ for the s-polarization. The angle is determined by Snell's law.

The reflectivity is $R = |r|^2$, with

$$r = \frac{n_{air}(M_{11} + n_{sub}M_{12}) - (M_{21} + M_{22}n_{sub})}{n_{air}(M_{11} + n_{sub}M_{12}) + (M_{21} + M_{22}n_{sub})}. \quad (5)$$

The reflectivity has been calculated as the average between the components parallel (p) and perpendicular (s) to the plane of incidence.

Since the materials are absorbing, the complex refractive index $n_j = \mathbf{n} - i\mathbf{k}$ has been considered. For the calculations, for each layer of the system, we have evaluated the refractive index as $\mathbf{n} = \mathrm{Re}\{\sqrt{\varepsilon}\}$ and $\mathbf{k} = \mathrm{Im}\{\sqrt{\varepsilon}\}$. The values used in the calculations for the pure materials are reported in Table I.

Starting from the dielectric function of pure materials, we applied the effective medium approximation to evaluate the effective dielectric function according to Eq. (1). Figure 3(a) shows the reflectivity vs excess Ge volume fraction, calculated using Eq. (3). We considered a 40 nm thick crystalline film (black solid line), in which both GST and Ge are crystalline, and a 40 nm amorphous GST film within which Ge crystalline grains are embedded (red solid line). These two cases correspond to the material before laser irradiation and to the sample L2, after irradiation at 1.5 J/cm^2, respectively. The calculated values are in good agreement with the reflectivity measured after amorphization in the L2 sample [Fig. 2(a), red symbols].

TABLE I. Parameters used in the calculations for all the involved materials.

Material	ε (at 790 nm)	Reference
SiO_2	2.17	15
Si (crystalline)	13.8 + 0.057i	16
Ge (crystalline)	22.56 + 3.29i	16
$Ge_2Sb_2Te_5$ (rock salt)	8 + 20i	17
$Ge_2Sb_2Te_5$ (amorphous)	7 + 10i	18

For sample L1, in which after laser irradiation, there is 20 nm of an amorphous film on top of a 20 nm thick crystalline film, the matrix element adopted in the calculations is

$$M = M_{SiO_2} M_{GST(am)} M_{GST(cry)}. \quad (6)$$

Since after melting and quenching, outdiffusion of Ge from the molten region has been observed, as reported in previous work,[7] the amorphous layer at the surface exhibits a lower Ge content, while the bottom crystalline film has a higher Ge fraction. The effect of compositional variations upon melting and quenching has been evaluated by starting with a 50% of excess Ge content (as in the as prepared film) and considering a depletion X of Ge in the amorphous, corresponding to the same increase X of Ge in the crystalline bottom layer. Figure 3(b) shows the reflectivity calculated by using Eq. (6) as a function of Ge reduction in the amorphous layer, assuming a 20 nm amorphous film on 20 nm crystalline film. For X = 0, there is no compositional variation between amorphous and crystalline film (i.e., excess Ge 50%). As the Ge content in the amorphous layer decreases, the reflectivity increases. The reflectivity is maximum for the maximum depletion, X = 50%, for which all the excess Ge in the amorphous film is segregated into the bottom crystalline film, and, therefore, the corresponding composition of the amorphous surface layer is GST225.

Once we have calculated the reflectivity as a function of excess Ge in the amorphous film, either with or without Ge content variation upon melting, we applied again the effective medium approximation to describe the evolution of the reflectivity upon crystallization, by considering the formation of GST225 crystalline grains in the hosting amorphous matrix. In this case, the crystal volume fraction is X_c and the effective dielectric function is

$$\varepsilon_{cry-eff} = 1/4\{2\varepsilon_p - \varepsilon'_p + \sqrt{[(2\varepsilon_p - \varepsilon'_p)^2 + 8\varepsilon_0\varepsilon_d]}\}, \quad (7)$$

with $\varepsilon_p = (1 - X_c)\varepsilon_{am\_eff} + X_c\ \varepsilon_{cry}$ and $\varepsilon'_p = X_c\ \varepsilon_{am\_eff} + (1 - X_c)\ \varepsilon_{cry}$, where ε_{cry} is the dielectric function of GST225 in the rock salt phase and ε_{am_eff} is the effective dielectric function of the amorphous phase, containing a given amount of excess Ge.

Figure 4 shows the reflectivity calculated as a function of the crystalline fraction (y axis) and of the excess Ge in the amorphous phase (x axis) for a 40 nm thick amorphous film [Fig. 4(a)] and for a 20 nm amorphous layer on 20 nm crystalline film, with different Ge amount (total excess Ge 50%) [Fig. 4(b)].

In the case of a uniform composition, Fig. 4(a) shows a calculated reflectivity of 0.42 for the amorphous phase. This value is in good agreement with the experimentally measured reflectivity, shown in Fig. 2(a) as red symbols, for sample L2, with 50% excess Ge and no compositional variation. However, the calculated reflectivity for the crystalline phase (0.54) is higher than experimentally measured; this may indicate that only partial crystallization is achieved upon annealing at 300 °C.

In the case of compositional variations upon melting, as occurring in sample L1, the measured reflectivity, shown in Fig. 2(a) as black symbols, is higher than that observed for the uniform film, both in the amorphous and in the crystalline phase. Such behavior is well predicted by the model: in Fig. 4(b), the

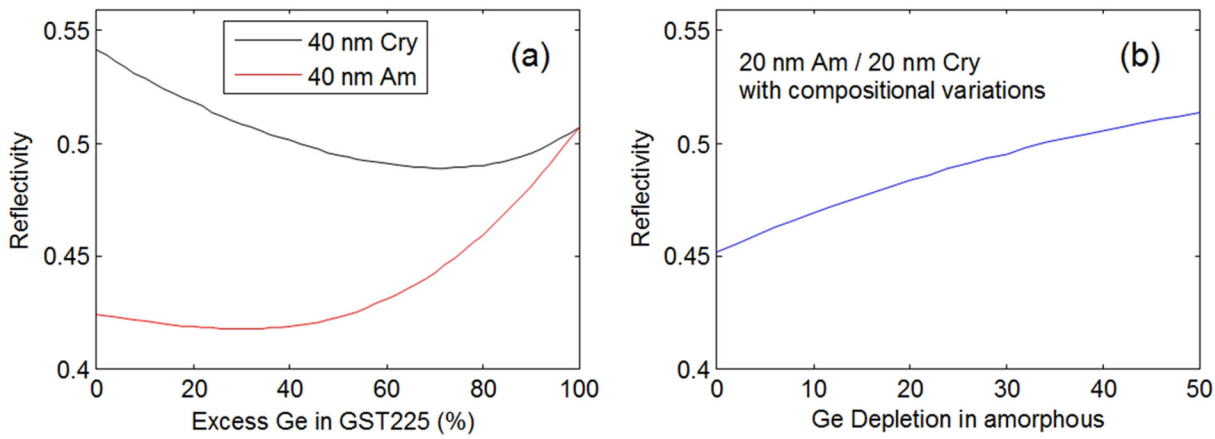

FIG. 3. (a) Calculated reflectivity as a function of excess Ge content in GST225 in the crystalline or in the amorphous phase, assuming no compositional variation upon melting. (b) Calculations with compositional variations upon melting and quenching. The reflectivity increases upon decreasing of excess Ge in the amorphous phase.

calculated reflectivity, taking into account for the compositional variation, is higher than that in Fig. 4(a). Moreover, the reflectivity value is modulated by the residual amount of Ge in the amorphous layer. By comparing the calculated values with the experimentally measured reflectivity, we may expect a residual excess Ge amount in the amorphous film in the range of 20%. These observations indicate that upon melting, even in the presence of a temperature gradient, producing segregation of the excess Ge in the cold regions, as in sample L1, the material still exhibits a good retention ability, with a crystallization temperature larger than 240 °C, i.e., well above the typical crystallization temperature of the composition GST225 (around 150 °C).

In order to get more information on the compositional variation occurring not only after melting and quenching but also during the crystallization, we performed TEM analyses on the annealed samples. Figure 5(a) shows a TEM micrograph of sample L2, after annealing up to 300 °C. In this case, the entire film thickness was melted and quenched by laser irradiation. The film is covered by a thin SiO_2 layer. Pre-existing crystalline Ge grains, formed during the first crystallization process, were not melted during laser irradiation, since the melting temperature of GST (~620 °C) is lower than that of pure Ge (938 °C). Figure 5(b) is a STEM micrograph in the dark field, showing the region that has been analyzed by EELS for the determination of the composition. The RGB image obtained by merging the elemental maps of Ge (blue component), Sb (green), and Te (red) obtained by EELS is shown in Fig. 5(c), with the corresponding extracted ternary phase diagram [Fig. 5(d)]. The average excess Ge in the film is 50% ± 4%.

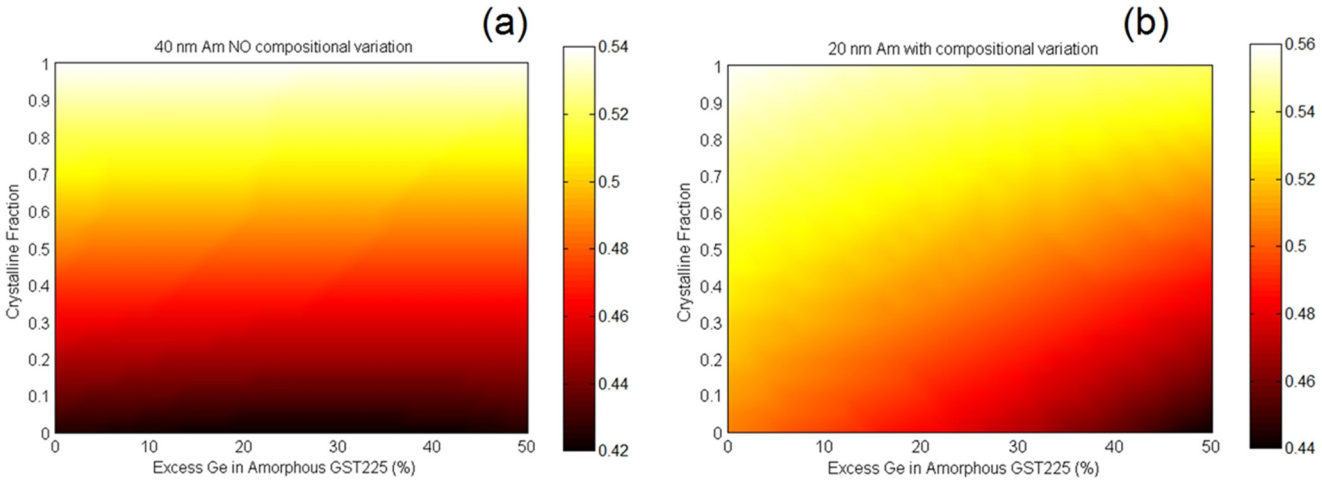

FIG. 4. Calculated reflectivity as a function of excess Ge content in amorphous GST225 and of the crystalline fraction: (a) 40 nm with no compositional variation upon melting. (b) 20 nm amorphous film with less Ge content than the 20 nm thick crystalline layer at the bottom.

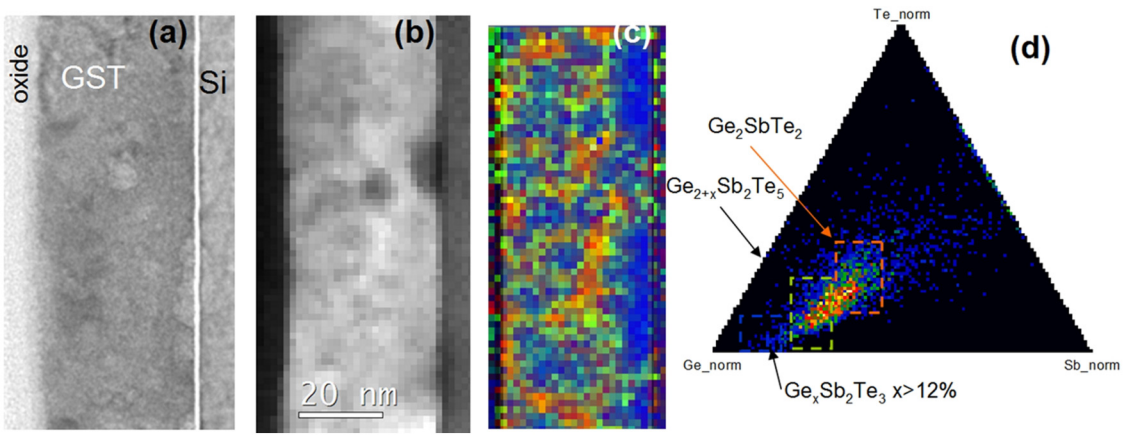

FIG. 5. TEM analysis in cross section of sample L2 after annealing up to 300 °C. (a) TEM micrograph in the bright field. (b) STEM micrograph of region in (a) the dark field. (c) Stoichiometric map extracted from EELS spectra acquired in each pixel, obtained by merging the Ge map (blue), the Sb map (green), and the Te map (red). (d) Extracted compositions in the ternary GeSbTe phase diagram.

The crystalline sample exhibits small Ge-rich regions, appearing in blue in Fig. 5(c), with a size of about 8 nm, corresponding to Ge crystalline grains embedded in the GST alloy. The regions surrounding the Ge grains may have composition $Ge_{2+x}Sb_2Te_5$, with $x \sim 5$, corresponding to excess Ge of 38%, compared to GST225, or close to GeTe, with some Sb doping, shown in orange. Therefore, in general, after crystallization, the material largely retains the excess Ge, with a slight tendency to phase separation.

Figure 6(a) shows the TEM micrograph of sample L1, after annealing up to 300 °C. Prior to the annealing, after melting and quenching by laser irradiation, the bottom part of the film, close to the interface with the Si substrate, was already crystalline and with a higher Ge content, while only the upper part was amorphous, with less Ge. Pre-existing crystalline Ge grains, not melted during laser irradiation, tend to accumulate in the bottom part of the film. Figure 6(b) shows the dark field micrograph of the same region

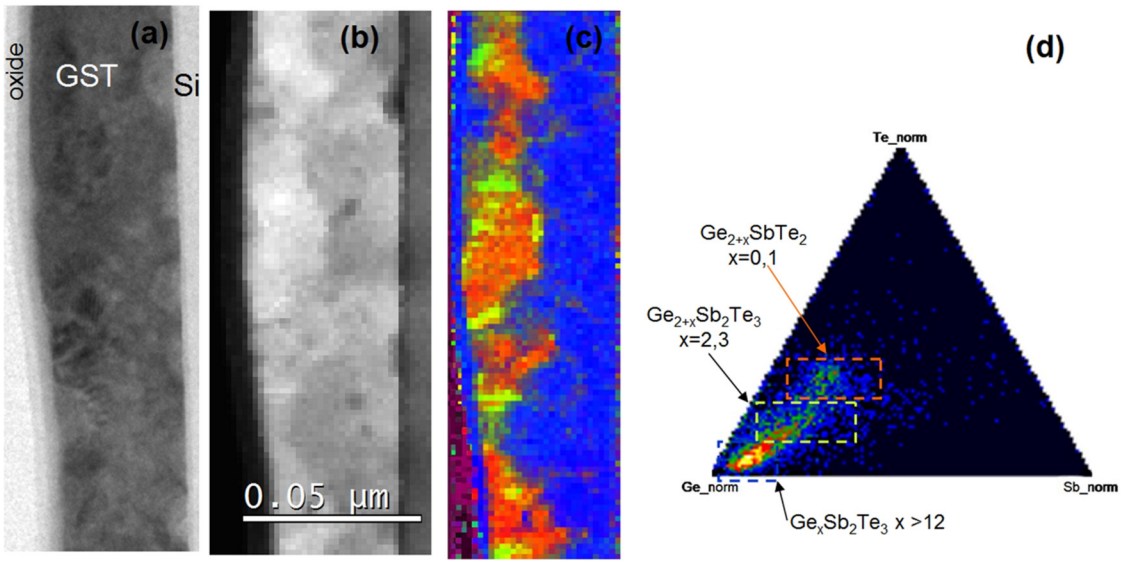

FIG. 6. TEM analysis in cross section of sample L1 after annealing up to 300 °C. (a) TEM micrograph in the bright field. (b) STEM micrograph of region in (a) the dark field. (c) Stoichiometric map extracted from EELS spectra acquired in each pixel, obtained by merging the Ge map (blue), the Sb map (green), and the Te map (red). (d) Extracted compositions in the ternary GeSbTe phase diagram. The blue region, mainly in the bottom part of the film, contains a large amount of Ge, of the order of 80%.

observed in Fig. 6(a), in STEM condition, used to perform the EELS analysis for the determination of the composition. Several regions have been analyzed by EELS, obtaining the elemental maps of Ge, Sb, and Te. Figure 6(c) shows, as an example, the RGB image obtained by the merging the elemental maps of Ge (blue), Sb (green), and Te (red), obtained in the region shown in Fig. 6(b). Compared to the GST225 composition, with 22% of Ge, the average excess Ge content calculated across the entire film thickness is 47% ± 3%. In contrast to the observations for sample L2, no clear crystalline Ge grains can be distinguished in the upper part of sample L1. This is mainly due to the Ge segregation in the bottom part of the film, which occurred during melting and quenching. As a consequence, the average Ge amount in the bottom part of the film [regions in blue in Fig. 6(c)] is 85% ± 5%. Therefore, the bottom part of L1 is mainly an almost continuous layer of Ge, mixed with GST. On average, compared to GST225, in the bottom part, the excess Ge after crystallization is larger than 60%. The upper part, instead, has an average Ge amount on the order of 38% ± 3% and therefore with about 16% of excess Ge. Such a result is in agreement with the expectation according to the reflectivity measurements and modeling. Moreover, in the upper part, different regions can be distinguished, corresponding to grains with different compositions. In order to determine the distribution of the compositions, a ternary phase diagram has been extracted, as shown in Fig. 6(d), and the compositions have been related to the colors appearing in Fig. 6(c). Regions in blue in Fig. 6(c) correspond to compositions $Ge_xSb_2Te_3$ with a total Ge amount of about 80%. Large grains, shown in orange, exhibit compositions $Ge_{2+x}SbTe_2$, with x = 0, 1, therefore suggesting the formation of GeTe, with inclusions of Sb and Ge. Smaller regions, mainly at the edges of the larger grains, shown in yellow/green, exhibit composition around $Ge_{2+x}Sb_2Te_3$, with x = 2,3. Although part of the excess Ge is segregated outside the amorphous region and the remaining excess Ge is only 16%, the crystallization temperature (245 °C), is considerably higher than that of GST225. Such a difference seems to be related to kinetic factors, since crystallization with phase separation involves long range diffusion of atomic species (mainly Ge), as well as to the formation of GeTe that, being characterized by high crystallization temperature (300 °C), may be crucial to assure the good data retention properties of Ge-rich GST alloys.

CONCLUSIONS

In conclusion, the crystallization process of Ge-rich GST thin film, after melting and quenching, has been studied by optical reflectance measurements and TEM. The optical properties can be successfully related to the structure and composition by means of the effective medium approximation. Two amorphization conditions were investigated. The first, obtained by using a laser energy density value able to melt the entire film thickness, preserves the initial distribution of excess Ge, giving rise to an amorphous film with excess Ge content of about 40%, compared to GST225 in which some crystalline Ge grains are embedded. The measured crystallization temperature is 275 °C and after crystallization only small regions exhibit phase separation, with GeTe formation, while the largest volume of the film is a Ge-rich GST225 alloy.

In the case of lower laser energy density, amorphization occurs only in the upper part of the film, with Ge segregation in the bottom crystalline region during melting. Despite containing a reduced amount of excess Ge (about 16%), crystallization of such a film occurs at 245 °C, with the formation of large grains with composition close to GeTe, surrounded by Ge-rich GST regions. The long range diffusion of Ge atoms, required for the crystallization process, seems to be key for the superior data retention properties of Ge-rich GeSbTe alloys.

ACKNOWLEDGMENTS

This project has received partial funding from the European Union's Horizon 2020 research and innovation programme under Grant Agreement No. 824957.

DATA AVAILABILITY STATEMENT

The data that support the findings of this study are available from the corresponding author upon reasonable request.

REFERENCES

[1]J. W. Burr *et al.*, "Phase change memory technology," J. Vac. Sci. Technol. B **28**, 223 (2010).
[2]S. Raoux, W. Wełnic, and D. Ielmini, "Phase change materials and their application to nonvolatile memories," Chem. Rev. **110**, 240–267 (2010).
[3]R. F. Freitas and W. W. Wilcke, IBM J. Res. Dev. **52**, 439 (2008).
[4]P. Zuliani *et al.*, Solid-State Electron. **111**, 27–31 (2015).
[5]V. Sousa *et al.*, in *Symposium on VLSI Technology (Digest of Technical Papers)* (IEEE, 2015), Vol. 7.4, p. T98.
[6]A. Kiouseloglou, G. Navarro, V. Sousa, A. Persico, A. Roule, A. Cabrini, G. Torelli, S. Maitrejean, G. Reimbold, B. De Salvo, F. Clermidy, and L. Perniola, "A novel programming technique to boost low-resistance state performance in Ge-rich GST phase change memory," IEEE Trans. Electron Devices **61**(5), 1246 (2014).
[7]S. Privitera, E. Rimini, and R. Zonca, App. Phys. Lett. **85**(15), 3044–3046 (2004).
[8]T. Li, L. Wu, X. Ji, Y. Zheng, G. Liu, Z. Song, J. Shi, M. Zhu, S. Song, and S. Feng, AIP Adv. **8**, 025201 (2018).
[9]S. M. S. Privitera *et al.*, J. Phys. D Appl. Phys. **51**, 145103 (2018).
[10]M. Agati, M. Vallet, S. Joulié, D. Benoit, and A. Claverie, J. Mater. Chem. C **7**, 8720 (2019).
[11]M.-C. Jung, Y. M. Lee, H.-D. Kim, M. G. Kim, H. J. Shin, K. H. Kim, S. A. Song, H. S. Jeong, C. H. Ko, and M. Han, "Ge nitride formation in N-doped amorphous $Ge_2Sb_2Te_5$," Appl. Phys. Lett. **91**, 083514 (2007).
[12]H. Horii *et al.*, in *A Novel Cell Technology Using N-doped GeSbTe Films for Phase Change RAM Symposium on VLSI Technology: Digest of Technical Papers 12B-5, Kyoto, Japan* (IEEE, 2003), p. 177.
[13]D. A. G. Bruggeman, Ann. Phys. **416**, 636 (1935).
[14]D.-H. Kim, F. Merget, M. Laurenzis, P. H. Bolivar, and H. Kurz, J. Appl. Phys. **97**, 083538 (2005).
[15]L. Gao, F. Lemarchand, and M. Lequime, "Refractive index determination of SiO_2 layer in the UV/Vis/NIR range: Spectrophotometric reverse engineering on single and bi-layer designs," J. Eur. Opt. Soc. Rapid Public **8**, 13010 (2013).
[16]D. E. Aspnes and A. A. Studna, Phys. Rev. B **27**, 985 (1983).
[17]J. Orava *et al.*, J. Appl. Phys. **104**, 043523 (2008).
[18]Z. Xu, C. Chen, Z. Wang, K. Wu, H. Chong, and H. Ye, "Optical constants acquisition and phase change properties of $Ge_2Sb_2Te_5$ thin films based on spectroscopy," RSC Adv. **8**, 21040 (2018).